JOURNAL OF MATERIALS SCIENCE 18 (1983) 793–803

Grain boundary Cr-depleted zones in Ti and Nb stabilized austenitic stainless steels

T. THORVALDSSON, G. L. DUNLOP
Department of Physics, Chalmers University of Technology, S-412 96 Göteborg, Sweden

The development of Cr-depleted zones due to the precipitation of $M_{23}C_6$ at grain boundaries during the ageing of niobium and titanium stabilized austenitic stainless steels (base composition Fe 17% Cr 12.5% Ni) at 750° C has been studied by STEM/EDX. The chromium composition profiles in high angle grain boundaries were found to be similar both in the vicinity of intergranular $M_{23}C_6$ carbides and at boundary segments between them, i.e. the whole grain boundary area acted as a collector plate to supply the growing $M_{23}C_6$ with chromium. Cr-depleted zones did not develop at coherent twin boundaries in the same way as at ordinary high angle boundaries. No major difference in the width or depth of the depleted zones was observed for the niobium and titanium stabilized alloys except for a weak persistence at 100 h in the niobium containing alloy. The error function solution of Fick's second law for diffusion was found to give a good approximation of the depleted zones in the early stages of ageing.

1. Introduction

It is generally believed that sensitivity to intergranular corrosion in austenitic stainless steels is caused by the intergranular precipitation of Cr-rich $M_{23}C_6$ grain boundary carbides [1, 2]. The formation of this carbide requires the diffusion of chromium towards the grain boundaries and thus causes a Cr-depleted zone to develop in the immediate vicinity of the boundary. This Cr-depletion model for sensitization was originally proposed by Bain *et al.* [2]. Refined thermodynamic and kinetic models based on the original assumptions of Bain *et al.* have been developed by Stawström and Hillert [3] and Tedmon *et al.* [4]. These models predict that the width of the Cr-depleted zones in practical cases in sensitized steels often are of the order of 500 nm or less.

Until recently no microanalytical methods have been available with sufficient spatial resolution to resolve such narrow regions. However, with the development of scanning transmission electron microscopy with energy dispersive X-ray spectrometry (STEM/EDX) this can now be accomplished on thin film specimens. Some recent work [5, 6] has already shown that the Cr-depleted zones which develop at grain boundaries in type 304 austenitic stainless steels have widths which are of the same order as those predicted by the models [3, 4].

Stabilized stainless steels contain additions of strong carbide forming elements such as titanium, niobium or vanadium which promote the precipitation of MC-type carbides rather than the formation of the considerably more Cr-rich $M_{23}C_6$ intergranular carbide. Thus, less $M_{23}C_6$ forms in stabilized steels and the tendency to form Cr-depleted zones is reduced. In addition, a precipitate hardening effect can be obtained if the MC carbides are uniformly distributed within the grains. This can be obtained by cold working the material prior to elevated temperature ageing in order to provide a network of dislocations for the MC carbides to precipitate on.

In the present work two austenitic stainless steels containing stabilizing additions of either titanium or niobium have been investigated by STEM/EDX in order to determine whether Cr-depleted zones formed during high temperature ageing. A major aim of the work was to determine if there was any substantial difference in the zones which developed when the stabilizing addition was either titanium or niobium. Earlier work on the same alloys has shown that there

0022–2461/83/030793–11$03.82/0

are substantial differences in their precipitation and coarsening behaviour [7, 8]. It was found that in the Nb-containing steel NbC was stable with respect to $M_{23}C_6$ at the ageing temperature of 750° C. However, contrary to normal expectations, the opposite behaviour occurred in the Ti-containing steel and TiC was replaced by $M_{23}C_6$ at long ageing times (about 5000 h).

2. Experimental details

The two experimental alloys had the same base composition (Fe 17% Cr, 12.5% Ni, 1.5% Mn and 0.5% Si) and approximately equi-atomic additions of carbon and either titanium or niobium, see Table I. The alloys were prepared by vacuum melting and hot forging. After solution treatment for 1 h at 1250° C followed by hot rolling and a further 15 min at 1250° C the alloys were quenched and deformed 5% in tension at room temperature. This deformation provided a suitable network of dislocations (density about $10^{14}\,m^{-2}$) for the nucleation of a fine dispersion of MC precipitates during the subsequent ageing treatments. Static ageing was carried out at 750° C on specimens in evacuated silica capsules which were water quenched after heat treatment. The grain sizes, measured by the linear intercept method, were 65 μm for the Ti-containing alloy and 50 μm for the Nb-containing alloy. Thin foils for transmission electron microscopy were prepared by jet polishing in 15% perchloric acid in methanol at −35° C and about 30 V. Carbon extraction replicas were obtained by etching in a solution of 12.5 g $CuCl_2$, 50 ml HCl and 50 ml ethanol at room temperature.

The metallographic examination was carried out in a JEOL 200 CX TEM/STEM microscope equipped with a Link energy dispersive X-ray spectrometer. All microanalyses were conducted using a graphite specimen holder. This combined with a specially inserted low background aperture resulted in a zero "in-hole" X-ray count. The compositions of intergranular $M_{23}C_6$ carbides were measured on extraction replicas whereas the composition profiles of chromium depleted zones were measured directly in thin foil specimens. The analyses were made quantitative by using the Link Systems RTS-2/FLS computer programme which uses a peak stripping routine and applies the Cliff–Lorimer [9] thin foil approximation with corrections for absorption [10].

The foil thickness was estimated by obtaining a two-beam condition and counting the thickness fringes from the edge of the specimen. This enabled the thickness to be determined to an accuracy of about 10 to 15% which was quite sufficient for the present purposes. Most analyses were obtained for a foil thickness of about 120 nm which meant that the absorption corrections were small (typically < 0.3 wt% for chromium).

The grain boundaries which were selected for composition profile measurements satisfied two criteria. Firstly, the plane of a chosen boundary was parallel to the electron beam when the foil was tilted to obtain maximum efficiency of detection for the X-rays. (This parallelism was experimentally possible to an accuracy of a few degrees.) Secondly, the chosen boundaries were radial to the central hole in the thin foil specimens. This increased the likelihood of obtaining constant foil thickness across the whole compositional profile. Each compositional profile was determined by making a series of point analyses at 25 nm intervals along a straight line perpendicular to the boundary. The incoming beam diameter was nominally 7 nm and analysis was carried out for 100 sec at each point.

3. Results

3.1. Microstructure

During ageing at 750° C MC precipitated rapidly on the dislocation network introduced by the 5% room temperature prestrain. $M_{23}C_6$ precipitated rapidly at the grain boundaries (Fig. 1). During the early stages of ageing the $M_{23}C_6$ continued to grow and decorated the grain boundaries with a centre-to-centre spacing which varied from boundary to boundary but was typically of the order of 0.2 μm. Volume fractions of $M_{23}C_6$

TABLE I Compositions of the titanium and niobium stabilized austenitic stainless steels (wt%)

Alloy	Composition						
	C	Mn	Si	Cr	Ni	Ti	Nb
Titanium stabilized	0.11	1.50	0.50	17.1	12.6	0.49	–
Niobium stabilized	0.11	1.49	0.50	17.5	12.5	–	0.74

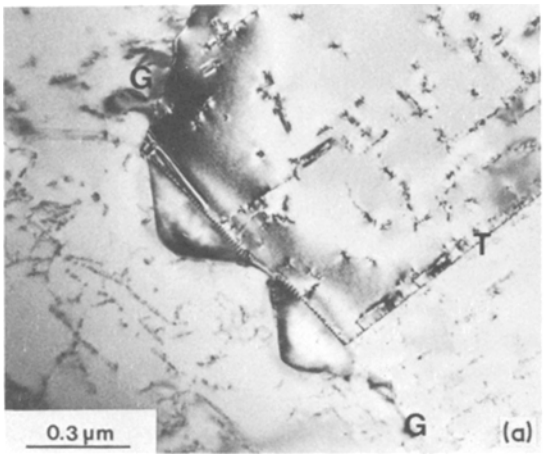

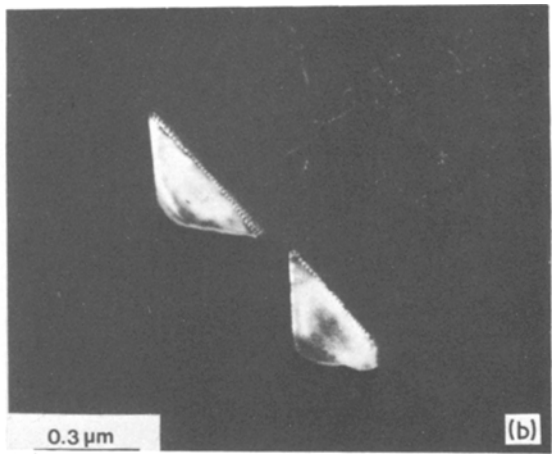

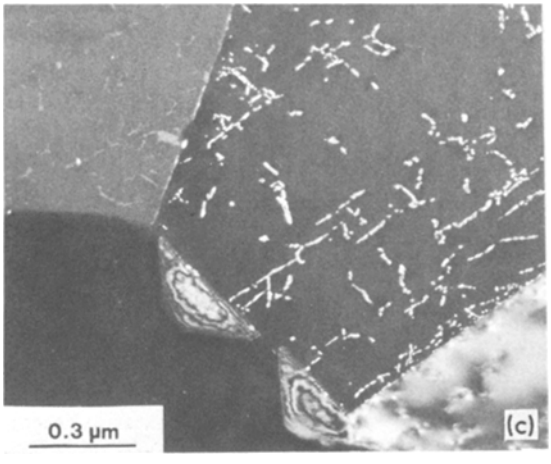

Figure 1 Precipitation of $M_{23}C_6$ and MC in the niobium stabilized steel after 8 h ageing at 750° C. (a) TEM bright field, high angle grain boundaries are indicated by G and a coherent twin boundary by T; (b) TEM dark field taken using a $M_{23}C_6$ reflection; (c) TEM dark field taken primarily with a MC reflections but also with a small contribution from a near-lying $M_{23}C_6$ reflection.

reported earlier for these two alloys [8] were 0.5% for the Ti-stabilized alloy and 0.9% for the Nb-stabilized alloy after 1170 h at 750° C.

3.2. Cr-depleted zones in the Ti-stabilized alloy

Concentration profiles from at least two different grain boundaries were determined for each ageing treatment. No significant variation was found between individual grain boundaries from the same heat treatment. The grain boundary concentration of chromium was determined on a large number of boundaries and was found to be constant within 2 wt % for each heat treatment. The bulk chromium concentration was found to vary slightly from grain to grain but the absolute decrease in chromium concentration was found not to vary between individual grain boundaries of the same heat treatment.

As shown in Fig. 2, no Cr-depletion could be detected at the grain boundaries after the original solution treatment followed by water quenching. During ageing at 750° C Cr-depleted zones developed in the vicinity of $M_{23}C_6$ carbides and also along segments of grain boundaries between $M_{23}C_6$ precipitates. Fig. 3 shows a typical area where composition profiles were determined at an $M_{23}C_6$ precipitate (see Fig. 5b) and away

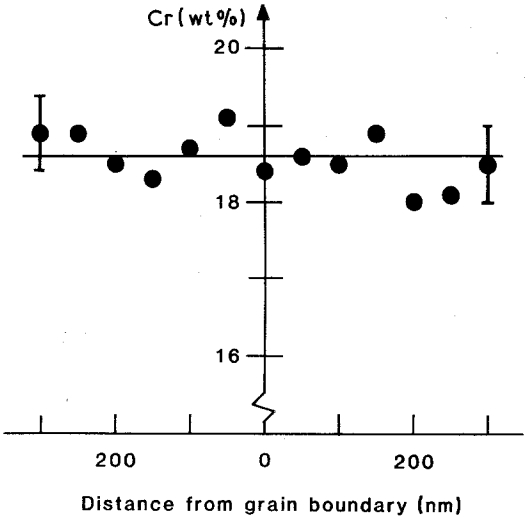

Figure 2 Chromium profile over a grain boundary in the titanium stabilized steel after solution treatment. The error bar indicates one standard deviation of the statistical counting error.

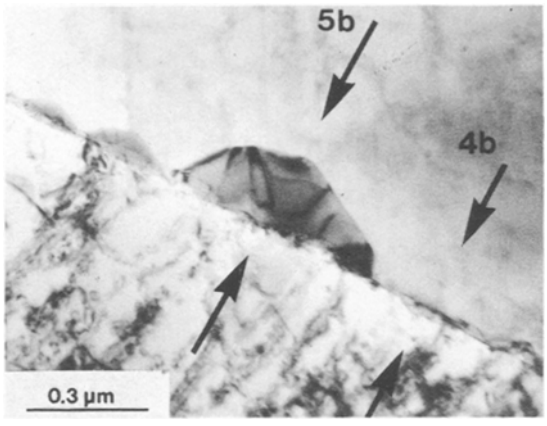

Figure 3 Typical area where composition profiles were obtained in the titanium stabilized steel. The arrows show the traces analysed in Figs. 4b and 5b. TEM bright field after 8 h ageing at 750° C.

from any precipitate (see Fig. 4b). The development and healing of Cr-depleted zones at segments of grain boundaries between $M_{23}C_6$ precipitates is shown as a function of ageing time in Fig. 4. The corresponding sequence of events at an $M_{23}C_6$ precipitate is shown in Fig. 5. In both cases the Cr-depleted zones formed and healed completely within 100 h at 750° C.

As a consequence of the spreading of the electron beam in the thin foil specimens the composition profiles of the Cr-depleted zones were easier to determine at grain boundary segments between $M_{23}C_6$ precipitates. The full widths of the zones were the same both at and between $M_{23}C_6$ carbides and developed from a full width of about 200 nm after 1 h to about 500 nm after 8 h. For these two ageing times, the measured Cr-content in the boundaries was about the same (14 to 15 wt %). No variation in Cr-content was observed along the grain boundaries between the $M_{23}C_6$ carbides. It can be noted that it was often observed that the profiles of the depleted zones were not exactly symmetrical. The magnitude of these variations could not be accounted for by possible differences in foil thickness across the measured traces and may possibly be interpreted as an effect of crystallographic orientation on the rate of diffusion.

As the Cr-concentration decreased towards the grain boundaries the iron and nickel contents increased correspondingly with the widths of the affected zones being the same for all three elements (see Fig. 6).

3.3. Cr-depleted zones in the Nb-stabilized alloy

Cr-depletion profiles for three ageing times for the Nb-stabilized alloy are shown in Fig. 7. For ageing times of 1 and 8 h the full widths were the same as for the titanium alloy (i.e. 200 and 500 nm). The measured Cr-contents of the grain boundaries were slightly lower (12 to 13 at %) than for the Ti-stabilized alloy but the decrease in chromium content from bulk composition was the same, i.e. 5 wt %. Contrary to the Ti-stabilized alloy, Cr-depleted zones could still be detected after 100 h at 750° C. At this ageing time the profile was very shallow with a boundary composition of 16.5 wt % Cr and a full width of 600 nm.

As for the Ti alloy the Cr-depleted zones were of a similar width both at $M_{23}C_6$ carbides and at grain boundary segments between carbide particles. No variation in grain boundary chromium concentration was found along the grain boundaries between carbides.

3.4. Compositions of the $M_{23}C_6$ carbides

Since in most cases the $M_{23}C_6$ carbides did not penetrate entirely through the thin foil specimens, their compositions were more satisfactorily determined on carbon extraction replicas. The only disadvantage here was that no composition could be obtained from the precipitates on grain boundaries where composition profiles were obtained. A total of 15 $M_{23}C_6$ precipitates, situated on three different grain boundaries, were analysed for each heat treatment condition. As shown in Fig. 8 the spread in compositions between different precipitates was very small for each ageing time. The $M_{23}C_6$ carbides contained considerable amounts of iron and nickel in addition to chromium. It can be seen in Fig. 8 that the concentration of all three elements changed with ageing time but there was no significant difference between the two alloys.

3.5. Cr depletion in the vicinity of twin boundaries

In the previous sections only ordinary high angle boundaries have been considered. $M_{23}C_6$ did not precipitate at coherent twin boundaries and no Cr-depletion could be detected at these interfaces. However, incoherent twin boundaries acted in the same way as ordinary high angle grain boundaries. $M_{23}C_6$ precipitated on these interfaces and Cr-depleted zones could be detected

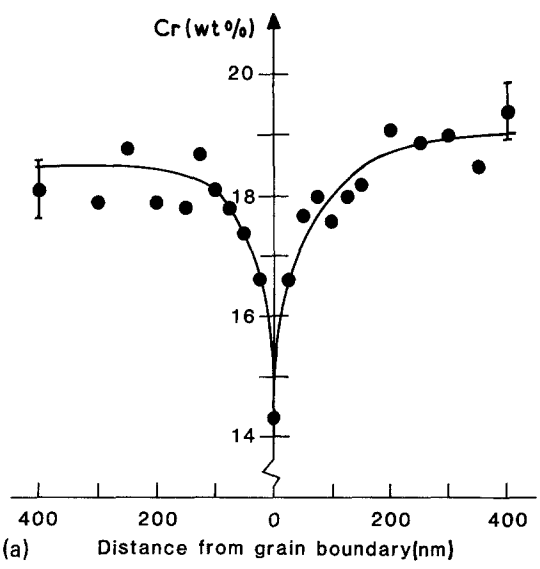

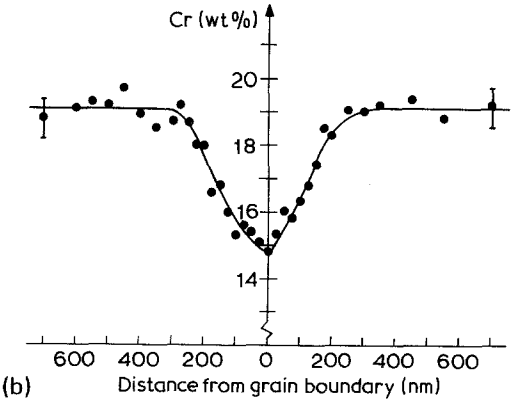

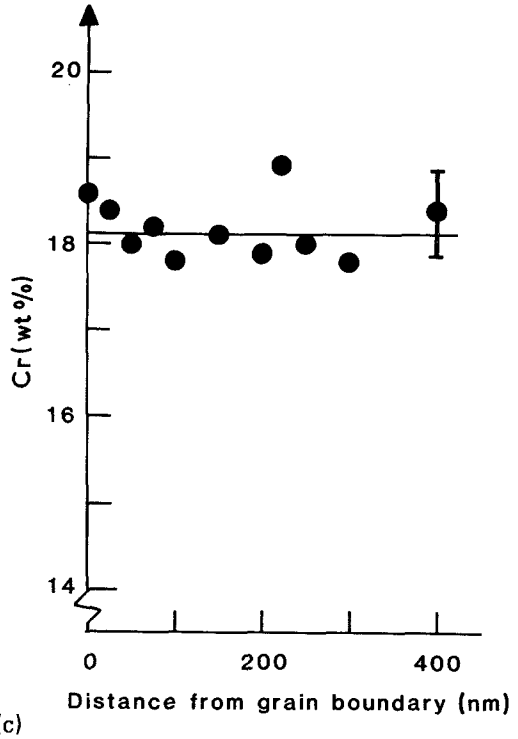

Figure 4 Chromium composition profiles over grain boundary segments between $M_{23}C_6$ precipitates in the titanium stabilized steel. (a) 1 h at 750° C; (b) 8 h at 750° C; (c) 100 h at 750° C.

(Fig. 9). The composition profile of these zones was the same as for general grain boundaries.

4. Discussion

4.1. Microstructure

Despite the fact that equi-atomic additions of titanium (or niobium) and carbon were made to these alloys, full stabilization against $M_{23}C_6$ precipitation was not achieved. This is not surprising since the precipitation of $M_{23}C_6$ never seems to be fully suppressed; even in strongly overstabilized alloys [11–14]. The rate of carbide precipitation varied between the two alloys. It has been found that the amount of $M_{23}C_6$ precipitated in the Nb-containing alloy is considerably greater than for the Ti-containing alloy for times up to 1170 h at 750° C [8]. At long ageing times (5000 h), far beyond that considered here, the situation changes and it has been found that $M_{23}C_6$ is replaced by NbC while the opposite occurs in the Ti-containing alloy (i.e. TiC transforms to $M_{23}C_6$) [8]. It is doubtful if this question of long term stability can have any influence on the development and healing of the Cr-depleted zones which occurs during the first 100 h of ageing at 750° C.

4.2. Development of Cr-depleted zones

The most striking feature in the compositional profiles presented in Figs. 4 and 7 is the similarity of the Cr-depleted zones between the two alloys for ageing times of 1 and 8 h despite the different amounts of $M_{23}C_6$ precipitation. It is worth noting that the grain boundary compositions at 1 and 8 h were measured to be in the order of the lower limit of 12 to 14 wt % Cr which is generally considered to be necessary for good corrosion resistance [1]. Thus, both alloys are likely to be sensitive to intergranular corrosion in this condition. However, no corrosion testing has been carried out to test this point.

It must be stressed that each measured com-

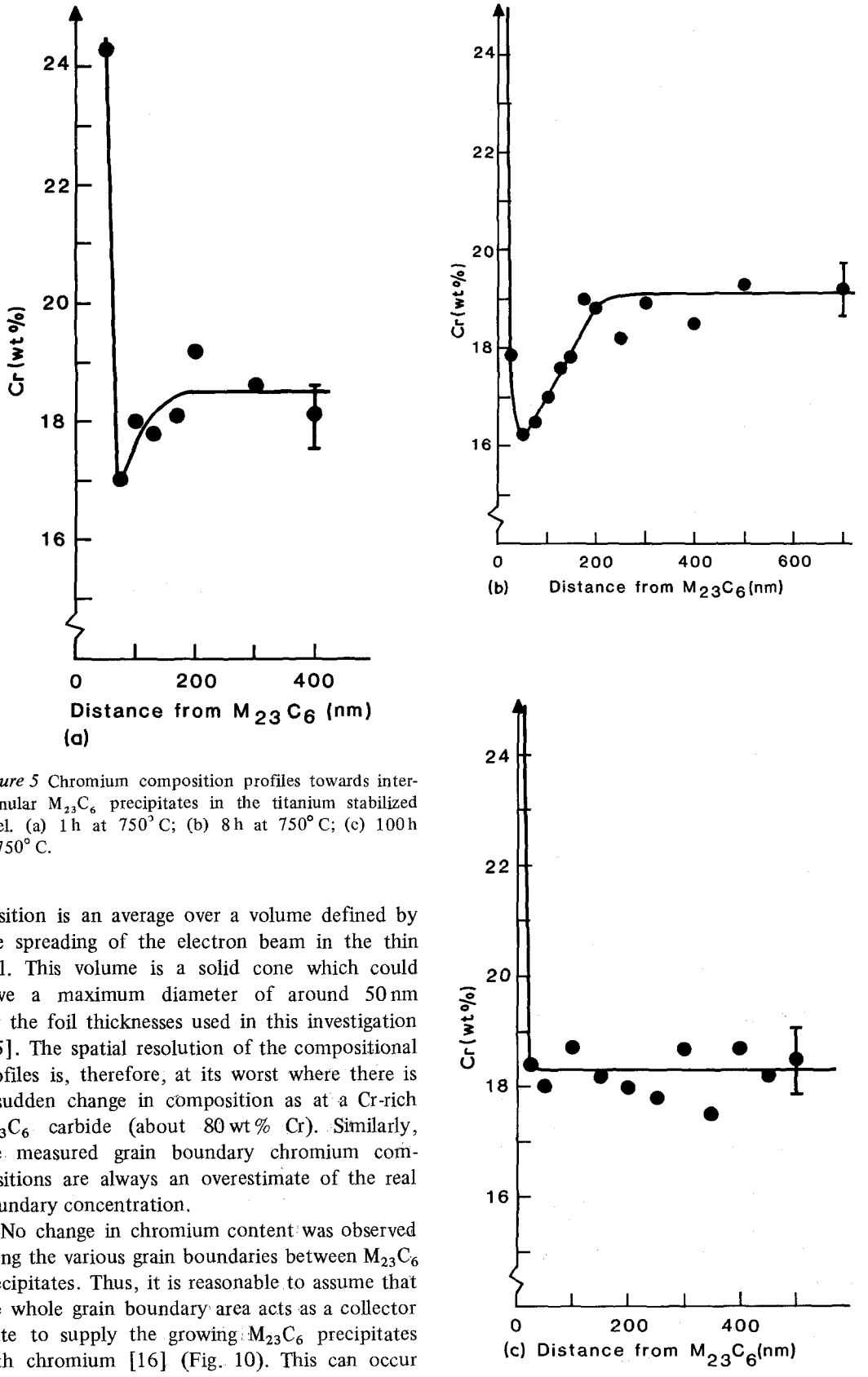

Figure 5 Chromium composition profiles towards intergranular $M_{23}C_6$ precipitates in the titanium stabilized steel. (a) 1 h at 750° C; (b) 8 h at 750° C; (c) 100 h at 750° C.

position is an average over a volume defined by the spreading of the electron beam in the thin foil. This volume is a solid cone which could have a maximum diameter of around 50 nm for the foil thicknesses used in this investigation [15]. The spatial resolution of the compositional profiles is, therefore, at its worst where there is a sudden change in composition as at a Cr-rich $M_{23}C_6$ carbide (about 80 wt% Cr). Similarly, the measured grain boundary chromium compositions are always an overestimate of the real boundary concentration.

No change in chromium content was observed along the various grain boundaries between $M_{23}C_6$ precipitates. Thus, it is reasonable to assume that the whole grain boundary area acts as a collector plate to supply the growing $M_{23}C_6$ precipitates with chromium [16] (Fig. 10). This can occur

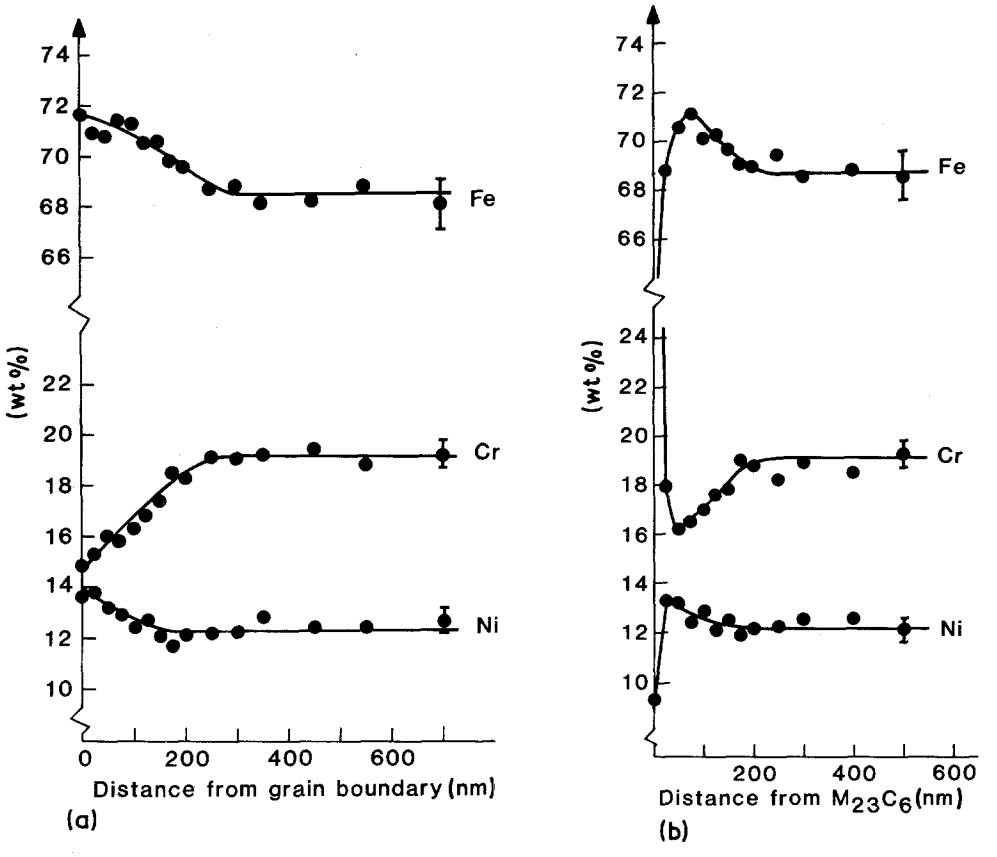

Figure 6 Iron, chromium and nickel composition profiles in the titanium stabilized steel after 8 h ageing at 750° C. (a) analysis toward grain boundary segments between $M_{23}C_6$ carbides; (b) analysis toward intergranular $M_{23}C_6$ carbide.

if the rate of chromium grain boundary diffusion is much faster than the corresponding rate of bulk diffusion.

4.3. Comparison with theoretical models

Since the chromium concentration is constant along the grain boundaries the simplest way to treat the development of Cr-depletion profiles is to use the following solution of Fick's second law for diffusion:

$$\frac{C_x - C_{gb}}{C_{bulk} - C_{gb}} = \text{erf}\ \frac{x}{2(Dt)^{1/2}}$$

where C_{gb} is the chromium concentration at either the grain boundary or at the matrix/$M_{23}C_6$ interface. C_{bulk} is the chromium concentration in the bulk and C_x is the concentration at distance x from the grain boundary. D is the volume diffusion coefficient and t is the ageing time. This solution involves a simplification of the real case since it is inherently assumed that chromium carbide is present on the boundaries at the beginning of ageing. Also no account is taken of the change in $M_{23}C_6$ composition with time.

A critical point when comparing measured profiles with this solution is the establishment of C_{gb} since this requires a method to deconvolute the effect of beam spreading in the thin foil. A satisfactory exact deconvolution procedure has yet to be established but Doig *et al.* [17, 18] have presented an approximate procedure involving curve fitting and beam broadening corrections (see Fig. 11). Figs. 12 and 13 show chromium depleted zones for the titanium alloy plotted in order to give the best fit to the error function solution (Equation 1). Best fit was obtained by choosing a suitable value for C_{gb}. The effect of beam spreading according to the model of Doig *et al.* is shown as a dotted line in Figs. 12 and 13. As can be seen the effect of spreading in the present work is quite small but is somewhat larger than predicted by the model (cf. Fig. 13).

A serious drawback with the simple error

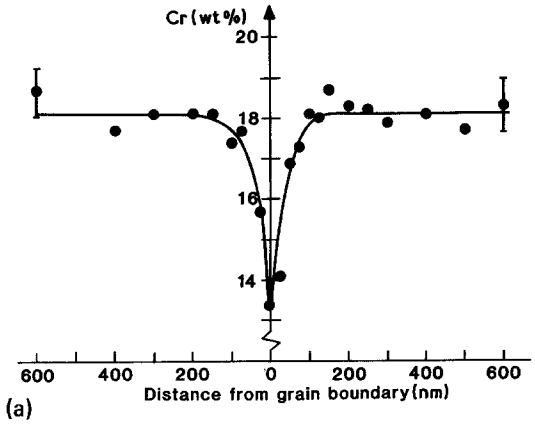

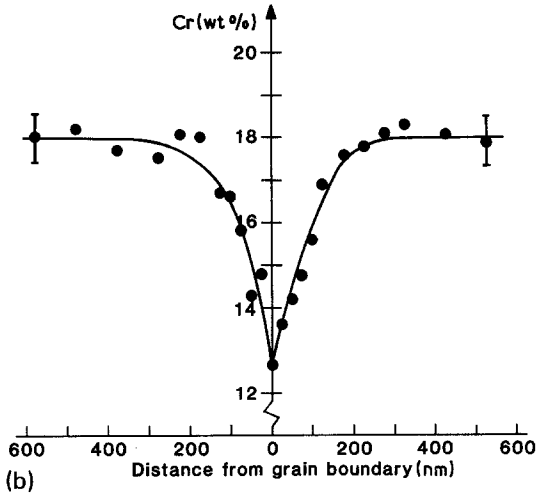

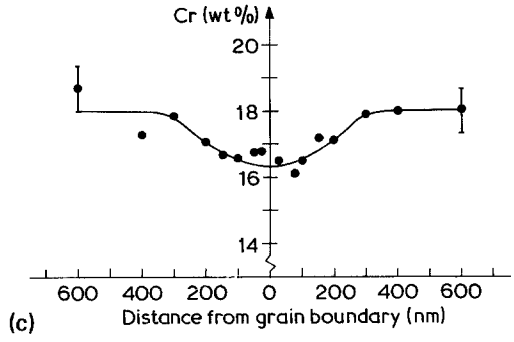

Figure 7 Chromium composition profiles over grain boundary segments between $M_{23}C_6$ carbides in the niobium stabilized steel (a) 1 h at 750° C; (b) 8 h at 750° C; (c) 100 h at 750° C.

function solution of the diffusion problem is that although good agreement can be obtained during rapid development of the depleted zones the model gives no explanation for their subsequent healing. The only way to obtain an explanation of this is to apply a thermodynamically based model. The only such model which has been published is that of Strawström and Hillert [3] in which the chromium concentration at the $M_{23}C_6$/matrix interface is given by local thermodynamic equilibrium. This model does not consider the effect of stabilizing additions and predicts

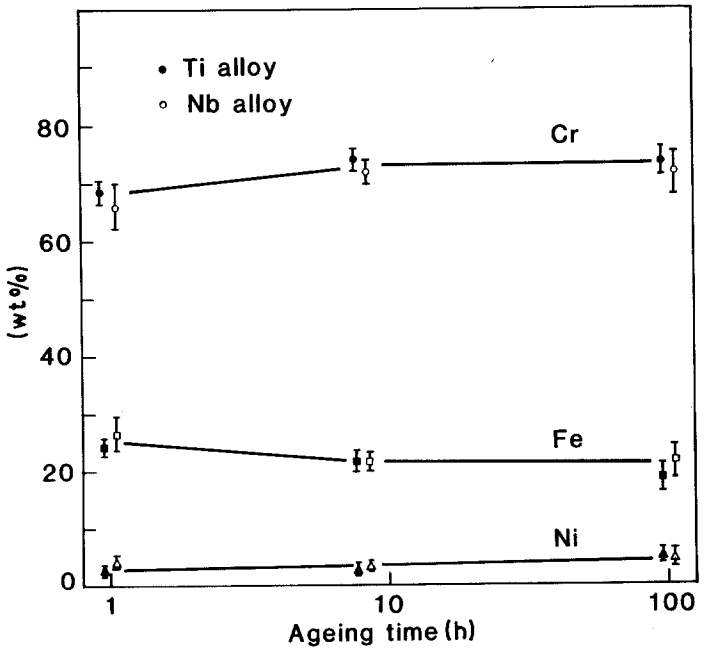

Figure 8 $M_{23}C_6$ composition as a function of ageing time. The error bars indicate one standard deviation of the spread between different measurements.

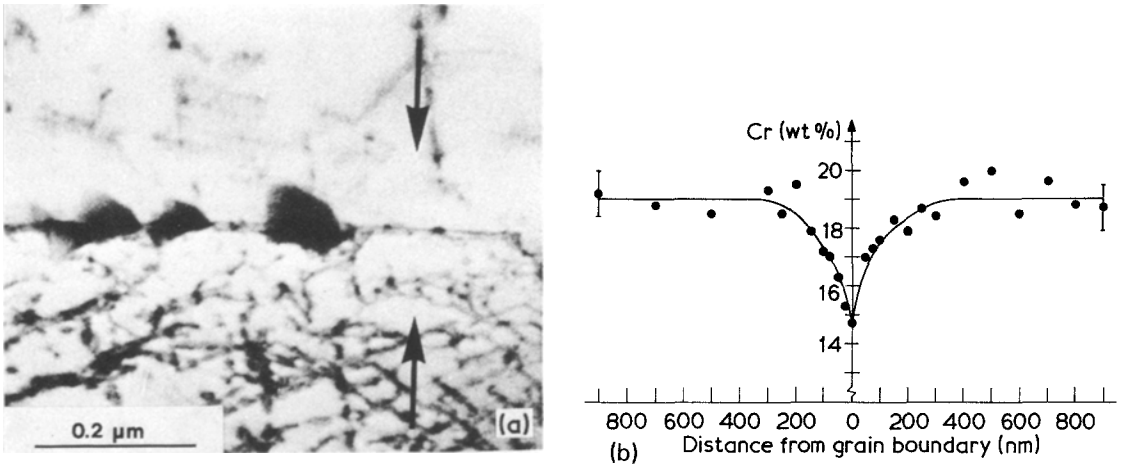

Figure 9 (a) $M_{23}C_6$ precipitation on an incoherent twin boundary in the niobium stabilized alloy after 8 h ageing at 750° C. STEM bright field; (b) chromium composition profile over the trace indicated above.

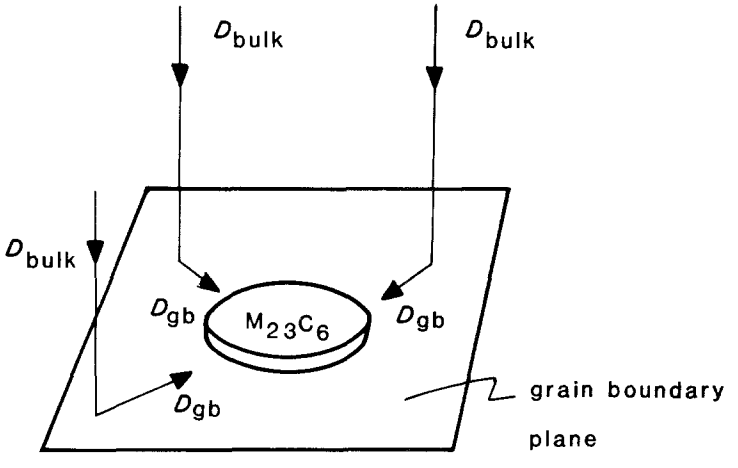

Figure 10 Schematic diagram of the collector plate model [16]. The whole grain boundary area acts as a collector plate to supply the growing $M_{23}C_6$ carbide with chromium.

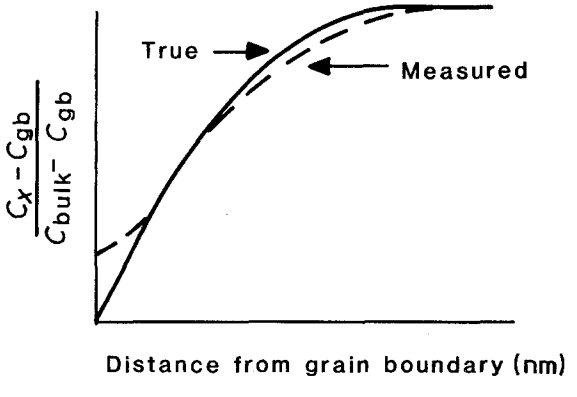

Figure 11 The influence of beam spreading on measured chromium concentrations (schematic diagram) according to Doig *et al.* [17, 18].

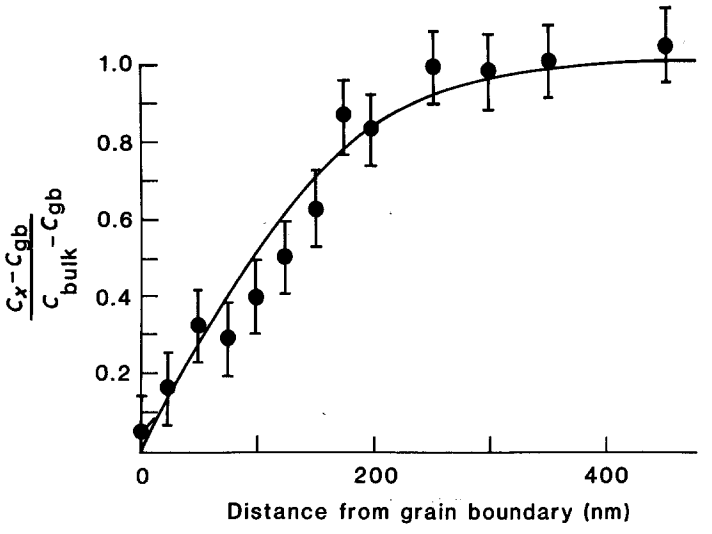

Figure 12 Normalized plot of half of the Cr-composition profile presented in Fig. 4b. The data has been fitted to an error function diffusion profile by finding the value of C_{gb} (14.5 %) which gave the best fit. The deviation in the expected profile due to beam broadening is indicated by the dashed line close to the grain boundary.

a healing time which is two orders of magnitude too long even if the carbon content of the alloy is reduced by the amount of carbon bound in MC precipitates. Thus it would seem that alloys with stabilizing additions are too complex to be treated by the original Stawström–Hillert model.

5. Conclusions

1. Cr-depleted zones can form at the grain boundaries of niobium and titanium stabilized austenitic stainless steels during ageing at 750° C.

2. The chromium profiles were similar in the vicinity of intergranular $M_{23}C_6$ precipitates and at boundary segments between precipitates. No variation was observed in the grain boundary chromium content between precipitates.

3. At this ageing temperature the whole grain boundary area acts as a collector plate to supply the growing $M_{23}C_6$ with chromium.

4. Cr-depleted zones do not form at coherent twin boundaries whereas the depleted zones which form at incoherent twin boundaries are the same as those which form at general grain boundaries.

5. Except for a weak persistence at 100 h for the Nb-stabilized alloy no major difference was noted in the width and depth of the Cr-depleted zones between the two alloys.

6. A good approximation to the formation of Cr-depleted zones at the early stages of ageing is given by fitting the results to the error function solution of Ficks second law.

Acknowledgements

The experimental alloys were prepared by Uddeholm AB. Financial support was received from the Swedish Board for Technical Development and the Swedish Natural Science Research Council. Discussions with P. Doig, P. R. Howell and A. Salwén are gratefully acknowledged.

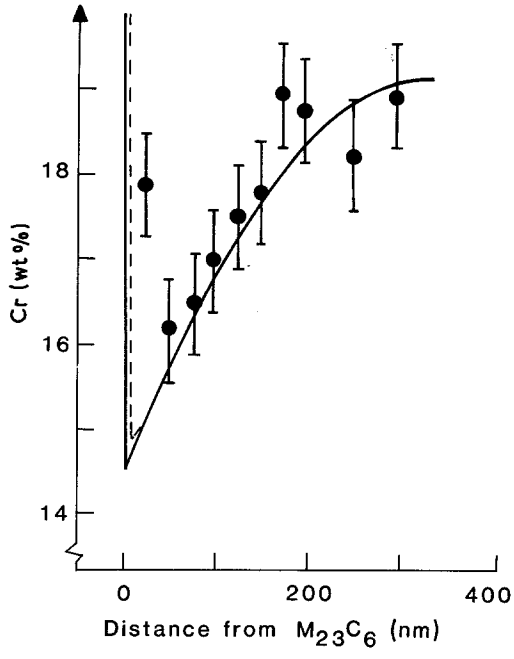

Figure 13 Comparison between the measured Cr-profile in Fig. 5b and the error function diffusion profile obtained from relevant diffusion data (19) together with a chosen value of C_{gb} (14.5 %) which gave the best fit. The deviation in the expected profile due to beam broadening is indicated by the dashed line close to the precipitate.

References

1. R. L. COWAN and C. S. TEDMON JR, "Advances in Corrosion Science and Technology" Vol. 3, edited by M. G. Fontana and R. W. Staehle (Plenum Press, New York, 1973) pp. 293.
2. E. C. BAIN, R. H. ABORN and J. J. B. RUTHERFORD, *Trans. Amer. Soc. Steel Treat.* **21** (1933) 481.
3. C. STAWSTRÖM and M. HILLERT, *J. Iron Steel Inst.* **207** (1969) 77.
4. C. S. TEDMON JR, D. A. VERMILYEA and J. H. ROSOLOWSKI, *J. Electrochem. Soc.* **118** (1971) 192.
5. C. S. PANDE, M. SUENAGA, B. VYAS, H. S. ISAACS and D. F. HARLING, *Scripta Metall* **11** (1977) 681.
6. M. G. LACKEY and F. J. HUMPHREYS, Proceedings of the 3rd International Conference on the Effect of Hydrogen on Behaviour of Materials, Moran, August 1980, Edited by I. M. Bernstein and A. W. Thompson (Metallurgical Society of AIME, 1981) p. 665.
7. T. THORVALDSSON and G. L. DUNLOP, *Met. Sci.* **14** (1980) 513.
8. *Idem ibid.* **16** (1982) 184.
9. G. CLIFF and G. W. LORIMER, *J. Microscopy* **103** (1975) 203.
10. J. I. GOLDSTEIN, J. L. COSTLEY, G. V. LORIMER and S. J. B. REED, "Scanning Electron Microscopy" Vol. 1 (IITRI, Chicago, 1977) p. 315.
11. T. SHINODA, T. ISHII, R. TANAKA, T. MIMINO, K. KINOSHITA and J. MINEGISHI, *Met. Trans.* **4** (1973) 1213.
12. J. M. SILCOCK, *J. Iron Steel Inst.* **201** (1963) 409.
13. P. W. TEARE and N. T. WILLIAMS, *ibid.* **201** (1963) 125.
14. J. M. SILCOCK, *ibid.* **211** (1973) 792.
15. J. I. GOLDSTEIN, "Introduction to Analytical Electron Microscopy", edited by J. J. Hren, J. I. Goldstein and D. C. Joy (Plenum Press, New York, 1979) p. 83.
16. H. B. AARON and H. J. AARONSON, *Acta Met.* **16** (1968) 789.
17. P. DOIG, D. LONSDALE and P. E. J. FLEWITT, *Phil. Mag. A* **41** (1980) 761.
18. *Idem,* Proceedings of the Conference on Quantitative microanalysis with high spatial resolution, Manchester, March 1981 (Metals Society, Manchester, 1981) p. 41.
19. R. A. PERKINS, R. A. PADGETT JR and N. K. TUNALI, *Met. Trans. A* **4** (1973) 2535.

Received 9 July
and accepted 19 July 1982